NAVAL POSTGRADUATE SCHOOL

MONTEREY, CALIFORNIA

THESIS

MULTI-SOURCE MFP WITH THE MULTI-VALUED BARTLETT PROCESSOR

by

Chungheon Lee

September 2023

Thesis Advisor: Kay L. Gemba
Co-Advisor: Woojae Seong,
Seoul National University

THIS PAGE INTENTIONALLY LEFT BLANK

REPORT DOCUMENTATION PAGE			*Form Approved OMB No. 0704-0188*

1. AGENCY USE ONLY *(Leave blank)*	**2. REPORT DATE** September 2023	**3. REPORT TYPE AND DATES COVERED** Master's thesis

4. TITLE AND SUBTITLE
MULTI-SOURCE MFP WITH THE MULTI-VALUED BARTLETT PROCESSOR

5. FUNDING NUMBERS

6. AUTHOR(S) Chungheon Lee

7. PERFORMING ORGANIZATION NAME(S) AND ADDRESS(ES)
Naval Postgraduate School
Monterey, CA 93943-5000

8. PERFORMING ORGANIZATION REPORT NUMBER

9. SPONSORING / MONITORING AGENCY NAME(S) AND ADDRESS(ES)
N/A

10. SPONSORING / MONITORING AGENCY REPORT NUMBER

11. SUPPLEMENTARY NOTES The views expressed in this thesis are those of the author and do not reflect the official policy or position of the Department of Defense or the U.S. Government.

12a. DISTRIBUTION / AVAILABILITY STATEMENT
Approved for public release. Distribution is unlimited.

12b. DISTRIBUTION CODE
A

13. ABSTRACT (maximum 200 words)

This study explores underwater source localization, focusing on matched field processing (MFP). The research identifies the challenges of localizing underwater sources and highlights MFP evolution and advantages. The aim is to comprehensively understand MFP, including its theoretical frameworks, algorithms, and mathematical representations. The methods employed offer insights into the performance of two processors through detailed explanations, simulations, and experimental data processing. The results demonstrate the advantage of the multi-valued Bartlett (MVB) processor over the Bartlett processor when localizing a weak signal to a strong signal in a challenging scenario. The study concludes with recommendations for further exploration and validation of advantages offered by the MVB processor, emphasizing its potential in identifying and localizing weak signals in complex, multi-source environments. We investigate averaging Bartlett with particular subspaces of the MVB processor on the dB scale. This inherently nonlinear technique significantly improved the localization of the weaker source, capitalizing on the distinct sidelobe configurations of the two processors. In conclusion, this research advocates for an extended exploration into the capabilities of the MVB processor. The spotlight remains on its promising potential to identify and pinpoint weak signals amid the intricate tapestry of multi-source underwater domains.

14. SUBJECT TERMS matched field processing, localization, shallow water			**15. NUMBER OF PAGES** 59
			16. PRICE CODE
17. SECURITY CLASSIFICATION OF REPORT Unclassified	**18. SECURITY CLASSIFICATION OF THIS PAGE** Unclassified	**19. SECURITY CLASSIFICATION OF ABSTRACT** Unclassified	**20. LIMITATION OF ABSTRACT** UU

NSN 7540-01-280-5500

Standard Form 298 (Rev. 2-89)
Prescribed by ANSI Std. 239-18

THIS PAGE INTENTIONALLY LEFT BLANK

Approved for public release. Distribution is unlimited.

MULTI-SOURCE MFP WITH THE MULTI-VALUED BARTLETT PROCESSOR

Chungheon Lee
Lieutenant Commander, Republic of Korea Navy
BA, ROK Naval Academy, 2013

Submitted in partial fulfillment of the
requirements for the degree of

MASTER OF SCIENCE IN ENGINEERING ACOUSTICS

from the

NAVAL POSTGRADUATE SCHOOL
September 2023

Approved by: Kay L. Gemba
Advisor

Woojae Seong
Co-Advisor

Oleg A. Godin
Chair, Department of Engineering Acoustics Academic Committee

THIS PAGE INTENTIONALLY LEFT BLANK

ABSTRACT

This study explores underwater source localization, focusing on matched field processing (MFP). The research identifies the challenges of localizing underwater sources and highlights MFP evolution and advantages. The aim is to comprehensively understand MFP, including its theoretical frameworks, algorithms, and mathematical representations. The methods employed offer insights into the performance of two processors through detailed explanations, simulations, and experimental data processing. The results demonstrate the advantage of the multi-valued Bartlett (MVB) processor over the Bartlett processor when localizing a weak signal to a strong signal in a challenging scenario. The study concludes with recommendations for further exploration and validation of advantages offered by the MVB processor, emphasizing its potential in identifying and localizing weak signals in complex, multi-source environments. We investigate averaging Bartlett with particular subspaces of the MVB processor on the dB scale. This inherently nonlinear technique significantly improved the localization of the weaker source, capitalizing on the distinct sidelobe configurations of the two processors. In conclusion, this research advocates for an extended exploration into the capabilities of the MVB processor. The spotlight remains on its promising potential to identify and pinpoint weak signals amid the intricate tapestry of multi-source underwater domains.

THIS PAGE INTENTIONALLY LEFT BLANK

Table of Contents

THIS PAGE INTENTIONALLY LEFT BLANK

List of Figures

List of Tables

THIS PAGE INTENTIONALLY LEFT BLANK

List of Acronyms and Abbreviations

FFT	fast Fourier transform
MFP	matched field processing
MVB	multi-valued Bartlett
SCM	sample covariance matrix
SNR	signal to noise ratio
SSR	signal to signal ratio
VLA	vertical line array

THIS PAGE INTENTIONALLY LEFT BLANK

Executive Summary

This research explores and enhances the methodologies used in underwater source localization with a primary focus on matched field processing (MFP). Recognizing the inherent challenges in pinpointing underwater source locations, the study compares the performance of two distinct processors: the Bartlett processor and the multi-valued Bartlett (MVB) processor.

The research framework we employed combines theoretical analysis, experimental simulations derived from the SWellEX-96 experiment, and real-world data processing. Both the Bartlett and MVB processors are extensively discussed, with the study providing mathematical representations, figures, and tables that underpin the analysis. Notably, our results show that the MVB processor demonstrates a superior capability for localizing weak sources, especially in the presence of a stronger counterpart, when juxtaposed with the Bartlett processor. An in-depth analysis reveals the strengths and weaknesses of each processor. Notably, the MVB processor outshines with reduced ambiguity and minimized sidelobes.

Validations from the simulations and real-world data processing using the SwellEx 96 data set further reinforce these findings. Intriguingly, for the MVB processor, there is a notable similarity in the partitioning of eigenvalues across frequencies. This attribute allows for incoherent averaging, which, in turn, augments the localization performance of the weaker source. To put it into perspective, the Bartlett processor demonstrated a marginal disparity of 0.5 dB between Source 2 and its peak sidelobe heights. Conversely, the MVB processor broadened this difference to a substantial 1.5 dB, thus highlighting its advanced capability in source localization.

Moreover, in an additional experiment, we averaged the Bartlett and MVB eigenvalue 2 (corresponding to the weaker Source) on the dB scale. This process is fundamentally a nonlinear operation and may amplify Source 2, given the distinct different sidelobe patterns of the two processors. While such averaging might not guarantee consistent results in all scenarios, it notably enhanced our study's localization of Source 2.

THIS PAGE INTENTIONALLY LEFT BLANK

Acknowledgments

I wish to express my profound gratitude to my advisor, Prof. Gemba. His consistent guidance, invaluable insights, and unwavering support have been the pillars of this research. Prof. Gemba's deep expertise and keen observations shaped and enriched every aspect of this work. I am also immensely thankful to my co-advisor, Prof. Seong. His contributions, encouragement, and expertise have been invaluable, and I sincerely appreciate his shared commitment to this journey. Both of them have been beacons of knowledge and inspiration, guiding me through the intricacies of this research. To the members of the USW group and the Physics and Electrical Engineering departments, I owe sincere thanks for our enlightening discussions that added depth to my research. I am deeply indebted to the dedicated staff of the NPS library; their unparalleled knowledge and patience in sourcing materials played an indispensable role in my research. The administrative and technical team of the Physics department deserve special mention. Their invaluable contribution to streamlining the logistics and ensuring the seamless execution of this work has been paramount. Every gesture of support, big or small, has not gone unnoticed and is profoundly appreciated. My family has been the backbone of this endeavor, providing relentless support, patience, and understanding during the most challenging moments. Their profound belief in my abilities fueled my perseverance. Lastly, I cannot express my thanks to my peers and friends. Their constant encouragement, emotional support, and constructive suggestions were constructive during this rigorous journey.

THIS PAGE INTENTIONALLY LEFT BLANK

CHAPTER 1:
Introduction

1.1 Source Localization

Ocean environments, with range-dependent sound speeds, multi-path propagation, scattering, and variable noise levels, make determining a submerged source's location difficult. It is crucial, however, to localize underwater sources for undersea warfare. matched field processing (MFP) refers to a "generalized plane-wave beamforming" [1] that compares the measured data at a vertical array of sensors to a replica derived by a full-field propagation model (solutions of the wave equation) for candidate source location to the same vertical array to localize an underwater source. A high correlation between the data and replicas indicates the location of the source [2], [3], [4], [5]. In Figure 1.1, the task of pinpointing the location of a submarine source in the ocean is illustrated. Assuming that the waveguide propagation model in this environment is adequately precise, the sounds that have been recorded are compared to a set of replicas. Through this comparison, the location of the submarine source (r, z) can ultimately be determined. The yellow peak signifies the position with the highest correlation, indicating the likely location of the submarine source.

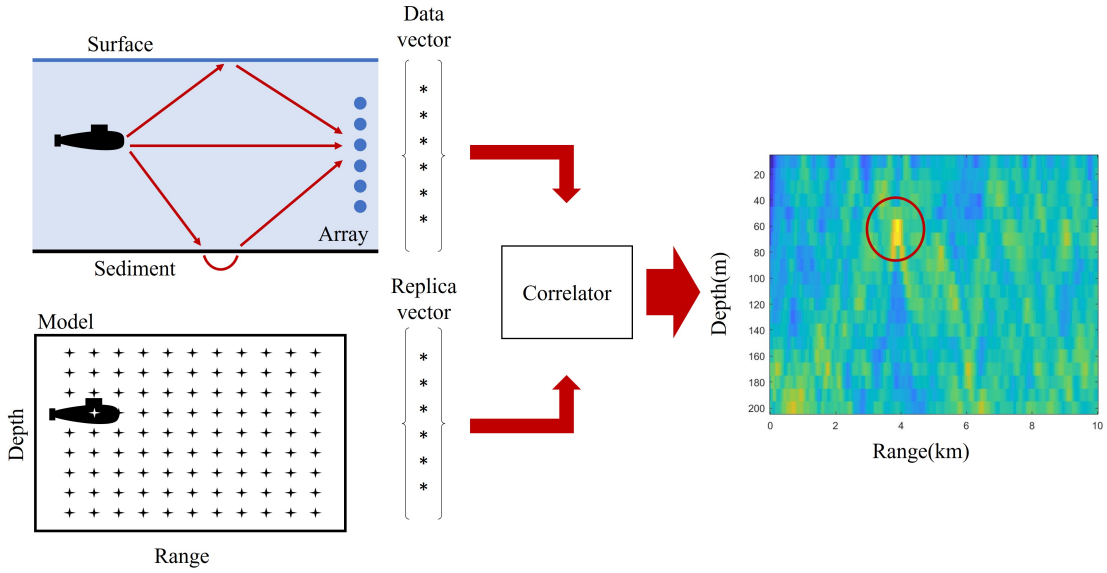

Figure 1.1. Matched field processing basic concept

1.1.1 Evolution of Matched Field Processing

Baggeroer et al. argue that the progression of (MFP) is closely linked with the advancements in acoustic propagation modeling within the ocean [6]. The connection between "waveguide models, arrays, and signal processing" was first recognized by Clay [7]. Hinich was the first to employ a vertical array for source localization [8]. Bucker was instrumental in developing MFP by employing realistic environmental models and creating what is known as the "conventional MFP " [9]. Klemm's introduction of "approximate orthogonal projection" marked the first instance of adaptive processing [1]. Bucker's concept was later utilized by Heitmeyer and others in 1983 during a workshop at the Naval Ocean Research and Development Agency [10]. Fizell and Wales were responsible for the initial experimental display of MFP with actual field data [11]. Additionally, Booth explained how broad-band signals had advantages in lowering sidelobes for precise source localization compared to MFP utilizing narrow-band signals, as demonstrated in Arctic experiments in deep and shallow waters [4]. The intricate nature of underwater acoustics, the requirement for exact detection and localization, the problems created by reverberation and multi-path interference, and the

potential for technological progress continue to fuel ongoing assessment and research in MFP within underwater acoustics.

1.1.2 Evolution of Matched Field Processing

Compared to plane wave beamforming, MFP offers several advantages. MFP provides an accurate model for signals within the ocean waveguide, reducing noise by discarding signals that do not align with the replicas [4]. The effectiveness of MFP is attributed to its integration of "the ocean environment, acoustic models, and array processing" to localize one or multiple sources in range and depth [1].

1.2 Challenges and Potential Solutions

MFP has a practical limitation, however. MFP is sensitive to mismatch since it uses a model of the ocean environment and requires receiver position information as input parameters [1], [12]. These parameters' uncertainties result in erroneous replica fields and higher sidelobes. This limits the utility of MFP for practical applications encountered in dynamic ocean environments. Therefore, dynamic ocean environments require robust processors. The Bartlett processor often deals with underwater acoustics problems because of the environmental mismatch [13]. The Bartlett processor provides a degree of robustness to environmental mismatch, yet it suffers from high-sidelobes. High-sidelobes are problematic as they can lead to false alarms and ambiguity, compromising the accuracy and reliability of the processing.

While remaining robust to environmental mismatch and improving localization performance, we investigate the utility of the multi-valued Bartlett (MVB) processor. The MVB processor combines the capability of the Eigen-processors to localize one or multiple sources separately while, when using all eigenvalues, it offers the same performance as the Bartlett processor. Unlike adaptive processors, its solution also offers some robustness to environmental mismatch. Since the MVB processor can localize multiple sources with different eigenvalues, we simulate a multi-source scenario with the SWellEx-96 experimental data set. The stronger source also is moving significantly. We compare processor performance with SWellEx-96 observations for single frequency (166 Hz) and multiple frequencies.

In Chapter 2, processors are introduced, and Chapter 3 provides a comprehensive data

selection and processing review. Simulations that examine processor performance in single and multi-source settings are presented in Chapter 4. We further explore the processor's performance in an identical situation with observations, using the SWellEx-96 data set [14], [15]. Chapter 4 wraps up with a discussion and summary, marking the conclusion of this thesis.

CHAPTER 2:
Matched Field Processing Procedure

2.1 Environmental Acoustics

Two standard wave equation approaches include Ray and Normal mode theory. The Ray and Normal mode theories are two fundamental theoretical frameworks used in underwater acoustics to explain sound wave propagation in the ocean. Ray theory is generally used for high-frequency (a few kHz or above) solutions, while Normal mode theory is applied at lower frequencies (below a kHz) [16]. The use of Ray theory is constrained by several factors [17]. In Brekhovskikh's study, the Ray theory does not apply in areas known as shadow zones or can be problematic in proximity to caustics. Moreover, Ray theory is unsuitable for low-frequency scenarios, where the sound's wavelength aligns with the vertical fluctuation of the sound speed or when only one mode is supported. Consequently, Brekhovskikh's study showed that for practical applications, one often has to turn to a different solution to the wave equation to address these issues. In such cases, analyzing the situation through normal modes proves more appropriate. Also, in Jensen's study [3], the physical interpretation benefits significantly from "the source image approach and other ray approaches" for high-frequency and transient propagation issues. The exact solution provided by the wavenumber integral, derived by contour integration, underscores the approximations made when utilizing Normal mode theory in imperfect waveguides where the modal expansion is not precise. The study is illustrated in the forthcoming section concerning the well-known Pekeris waveguide. Jensen's study also showed that the Normal mode theory employs "complex contour integration" to transform the integral expression into a sum of residues. In contrast, the wavenumber integration method directly computes the integrals using numerical quadrature.

2.1.1 Normal Modes

Pekeris was the pioneer in developing the theoretical framework for a fundamental two-layer ocean model [18]. The Normal mode theory is a theory for solving problems related to depth-dependent equations [3]. It involves addressing a non-driven version of the equation,

which can be resolved using the wavenumber integration technique. These two numerical techniques are intimately connected. The non-driven problem includes vibrating modes that resemble those of a vibrating string. According to Jensen, these vibration frequencies correspond to the horizontal wavenumbers integral to modal propagation. The same study indicates that the aggregate acoustic field is derived by combining the contributions of each mode. This compiled field is then adjusted based on the source depth. The Normal mode theory offers multiple advantages. Once its eigenvalue problem is addressed, the solution becomes universally applicable across various source and receiver configurations. Secondly, it accommodates moderately range-dependent scenarios with ease through the adiabatic approximation. Lastly, with added effort, it can also be tailored for highly range-dependent conditions via the coupled mode theory [19]. This approach, however, does not fully consider the near field [3].

In Jensen's study [3], the pressure in range and depth is calculated as follows

$$p(r,z) = \frac{i}{\rho(z_s)\sqrt{8\pi r}} e^{-i\pi/4} \sum_{m=1}^{\infty} \Psi_m(z_s)\Psi_m(z) \frac{e^{ik_{rm}r}}{\sqrt{k_{rm}}}, \tag{2.1}$$

where $\Psi_{\mathrm{m}}(\mathrm{z})$ symbolizes the particular function $\Psi(z)$ that is found with the modal wavenumbers k_{rm}. These modes are defined by both "a mode shape function" $\Psi_{\mathrm{m}}(\mathrm{z})$ and "a horizontal propagation constant k_{rm}." In this context, z represents the depth beneath the ocean surface, while the range r denotes "the horizontal distance" from a vertical array of hydrophones located at "$z = z_j$ for $1 \leq j \leq n$." The boundary conditions that are applied result in "a pressure-release surface at $z = 0$ and a rigid bottom at $z = D$."

2.1.2 KRAKEN

During the late 1970s, various normal-mode models were extensively employed to forecast acoustic transmission loss in the ocean. Each model, however, came with its own set of challenges. Common issues involved numerical instabilities for certain kinds of sound-speed profiles and an inability to compute a comprehensive set of ocean modes. Simply put, there was a demand for a robust and efficient model. The KRAKEN Normal mode model was created to address these issues. Initially, KRAKEN was developed as a research code to assess new algorithms, which meant it needed several modifications to function as a production code. This modification began at the Naval Ocean Systems Center and

was carried on at the Naval Research Laboratory to assist the research on matched-field processing. Now, KRAKEN is recommended for more experienced models and advanced scenarios. Figure 2.1 shows the KRAKEN Normal mode model for SWellEX-96 Event S5 at 166Hz with 21 and 64 elements, respectively. Designing an array to meet specific performance criteria requires a balance among various factors, including the array geometry, the number of sensors involved, and the signal to noise ratio (SNR) and signal-to-interference ratio. This array design involves trade-offs among these elements to achieve the desired performance [20]. The 61-element array provides more SNR but not more aperture because the array's length is the same. The 21-element array appears sufficient to compare the observed field to replicas generated with KRAKEN and will be used in this work.

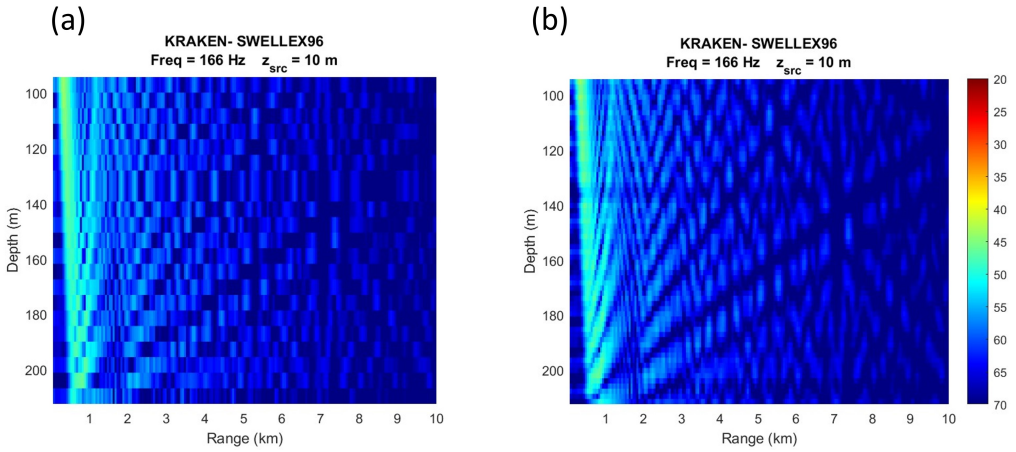

Figure 2.1. KRAKEN normal mode model for SWellEX-96 Event S5 at 166Hz: (a) 21 elements, (b) 64 elements. The 21 (64) elements are evenly spaced at 5.63m (1.875 m) across a 118.1-m aperture.

2.2 Processing Algorithms

2.2.1 Bartlett

The Bartlett processor in its quadratic form involves the data covariance matrix and the replica field [13]. Traditionally, the estimation of source location parameters has been

initiated using the Bartlett processor, serving as a starting point for this process [2].

The acoustic environmental model $\mathbf{a}(f_i, r, z)$ is calculated at the array in range and depth cell(r, z) in each frequency f_i. The replica vector, $\mathbf{w}(f_i, r, z)$, is a normalized vector of the environmental model $\mathbf{a}(f_i, r, z)$:

$$\mathbf{w}(f_i, r, z) = \frac{\mathbf{a}(f_i, r, z)}{\|\mathbf{a}(f_i, r, z)\|}. \tag{2.2}$$

We assume that the signal and noise are independent in estimating the sample covariance matrix (SCM). The term "snapshot" refers to a vector of complex numbers computed via fast Fourier transform (FFT). Its length is the same as the number of array elements. Using L snapshots, the SCM is denoted by $K \in \mathbb{C}^{\mathbb{N}\times\mathbb{N}}$ [2], and can be represented as

$$\hat{K} = \frac{1}{L}\sum_{l=1}^{L} \mathbf{d}_l \mathbf{d}_l^{\dagger}, \tag{2.3}$$

where † denotes complex conjugation.

The snapshot $\mathbf{d}_l \in \mathbb{C}^N$ is comprised of "a vector of Fourier coefficients at a single frequency f," gathered using a "FFT from the l-th data segment of each array element" [21]. Generally, it's beneficial and sometimes necessary to average over multiple snapshots to enhance the SNR, thereby improving source localization. The count of snapshots usable to determine $\hat{K}$ is influenced by the duration for which a source remains within a resolution cell [22], [23].

The output of the Bartlett processor is

$$B(f_i, r, z) = \mathbf{w}(f_i, r, z)^{\dagger} \hat{K} \mathbf{w}(f_i, r, z) = \frac{1}{L}\sum_{l=1}^{L} \left|\mathbf{w}^{\dagger}\mathbf{d}_l\right|^2. \tag{2.4}$$

Although the traditional linear Bartlett processor can handle environmental mismatches, it faces substantial challenges with sidelobes, which frequently cannot be differentiated from the main lobe [5]. The Bartlett processor does not invert $\hat{K}$. Therefore, there is no need for a "minimum number of snapshots," so it is susceptible to high-sidelobes [24]. Suppressing these sidelobes is vital, especially when dealing with multiple sources or a mix of sources

and interference [2].

The reduction in range/depth sidelobe levels was achieved by erratically averaging the processing output across multiple tones, facilitating precise identification and tracking of the source [4]. In the study conducted by Booth, the correlations among the multiple frequencies were averaged incoherently, producing a multi-tone correlation estimate:

$$\overline{B(r,z)} = \sum_{i=1}^{N_f} B(f_i, r, z), \tag{2.5}$$

where N_f denotes the number of frequencies.

2.2.2 Multi-Valued Bartlett

For problems involving multiple sources, the sidelobes may obscure weaker sources and make it difficult to decide how many sources are present. High-resolution beamformers that suppress sidelobes, such as eigen-processors, can often reduce this difficulty. As an eigen-processor, the MVB processor has an advantage over other adaptive processors. The MVB processor, which relates to the Bartlett processor, tends to be more forgiving when encountering imperfect environmental conditions, frequently met in practical applications. The MVB processor also proves beneficial in separating signals from noise [13]. The multi-valued Bartlett processor, an extension of the standard Bartlett processor, operates by excluding the influence of specific eigenvectors from the total sum [25]. In Collins' study, this technique is founded on the realization that energy from various sources often segregates into distinct eigenvectors. In simulations that include noise originating from a particular source, the MVB processor has shown enhanced performance compared to the traditional Bartlett processor. The study further revealed that the MVB processor operates on the premise that acoustic fields arising from sources at varying locations tend to lack spatial correlation on a hydrophone array, and, consequently, energy from various sources usually separates into other eigenvectors, which align with the largest eigenvalues. Therefore, the MVB processor efficiently identifies and maps the routes of multiple moving sources.

The MVP processor is constructed by decomposing the SCM into eigenvalues and eigen-

vectors:

$$\hat{K} = \frac{1}{L}\sum_{l=1}^{L} \mathbf{d}_l \mathbf{d}_l^{\dagger} = \sum_{j=1}^{n} \lambda_j \mathbf{v}_j \mathbf{v}_j^{\dagger}, \tag{2.6}$$

where λ_j is the j-th eigenvalue and $\mathbf{v}_j$ denotes the jth eigenvector. There is no reason to assume different sources are correlated; as a result, energy from these sources is partitioned into distinct eigenvectors. In distributed processes like ambient noise, energy spreads among multiple eigenvectors. This energy partitioning can enhance MFP performance when interference arises from multiple sources and noise [26].

We denote the MVB power output for the j-th eigenvalue and eigenvector combination by B_j. Note that B_j also is associated with the Bartlett processor [13]. The power output of the MVB processor is

$$B_j(f_i, r, z) = \mathbf{w}^{\dagger}(f_i, r, z) K_j \mathbf{w}(f_i, r, z) = \lambda_j \left| \mathbf{w}^{\dagger} \mathbf{v}_j \right|^2 . \tag{2.7}$$

Given that B_j only is associated with the j-th eigenvalues of the SCM, the relationship between the MVB and Bartlett processor is

$$B(f_i, r, z) = \sum_{j=1}^{n} B_j(f_i, r, z) = \sum_{j=1}^{n} \lambda_j \left| \mathbf{w}^{\dagger} \mathbf{v}_j \right|^2 . \tag{2.8}$$

For a broadband source, localization performance can improve by averaging the MVB B_j over multiple frequencies incoherently, assuming that eigenvalues and eigenvectors equally partition across frequencies.

The multiple-frequency MVB (for a single eigenvector and eigenvalue) is then given by

$$\overline{B_j(r, z)} = \sum_{i=1}^{N_f} B_j(f_i, r, z). \tag{2.9}$$

Similar to Equation 2.8, the relationship between the multiple frequency MVB and the

Bartlett processor is

$$\overline{B(r,z)} = \sum_{i=1}^{N_f} B(f_i, r, z) = \sum_{i=1}^{N_f} \sum_{j=1}^{n} B_j(f_i, r, z). \tag{2.10}$$

THIS PAGE INTENTIONALLY LEFT BLANK

CHAPTER 3:
Experimental Data

3.1 SWellEX-96 Data Set

3.1.1 Experimental Overview

The SWellEX-96 experiment was carried out in the coastal waters of San Diego, California, to simulate the localization of targets in shallow waters. The floating instrument platform deployed a vertical line array (VLA) comprising "64 calibrated hydrophone elements, evenly spaced at 1.875 m across a 118.1-m aperture and sampled at a frequency of 1500 Hz" [14]. We used the SWellEX-96 Event S5 data set for our analyses. Figure 3.1 traces the path of the source ship (R/V Sproul) moving from the south toward the VLA at a nominal speed of 5 knots (2.5 m/s) while towing a source at a depth of 60m. The transmission included numerous tonals with varying source levels, ranging from 49 Hz to 388 Hz. This particular collection of tonals is known as T-49-13. The T-49-13 tonal pattern comprises 5 sets of 13 tones, with each set spanning frequencies from 49Hz to 400Hz. The first set of 13 tones is released at the highest level, termed the "High Tonal Set," and these tones are projected with transmitted levels of around 158 dB. We use this set of tonals for processing (49, 64, 79, 94, 112, 130, 148, 166, 201, 235, 283, 338, 388Hz) [27]. Figure 3.2 presents the waveguide, illustrating its sound profile and "geo-acoustic parameters" for the "near-range-independent" SWellEx-96 Event S5. For range-independent processing, the water depth is considered equal to the water depth at the array, which is 216 m. The seafloor features a 23.5 m thick layer of sediment over an 800 m thick mudstone [2].

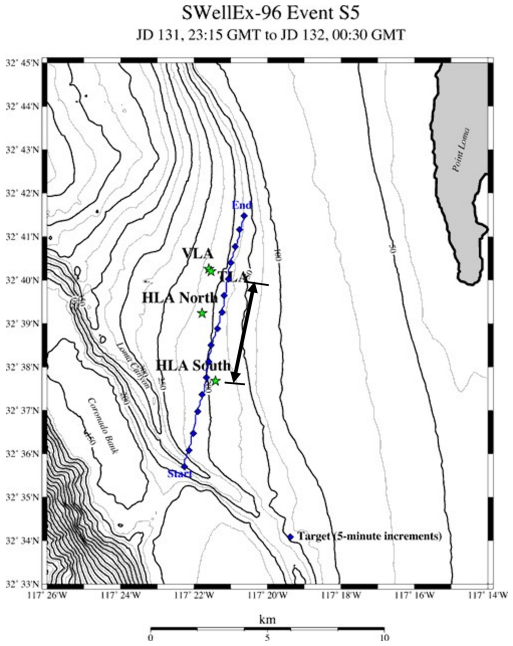

Figure 3.1. The trajectory of the R/V Sproul during the SWellEx-96 Event S5. The marked blue ship navigated along an approximate 200m isobath, towing a deep source at a depth close to 60m. The event was captured over 75 minutes by a VLA. We extract the data from 25 minutes to 55 minutes, and the legs are marked with the black arrow.

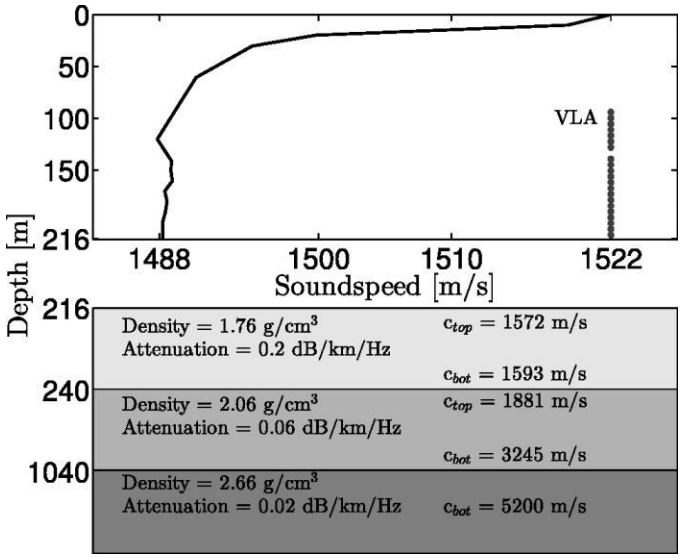

Figure 3.2. Waveguide with sound profile and geo-acoustic parameters about the range-independent SWellEx-96 Event S5. Source: [2] Assumptions have been made about the water depth in the waveguide, equating it to the water depth at the array for range-independent processing. The array geometry, representative of the one used during the SWellEx-96 experiment, comprises a 21-element array covering roughly 120 meters.

3.2 Multi-Source Simulation

To create a multi-source scenario, we duplicated the original SWellEX-96 data, setting two sources 2km apart and simulating the movement of one source over 300m. This distance was chosen to be similar to the approximate range resolution at 166 Hz for greater than the main lobe, as shown in Tables 3.1 and 3.2. MFP uses "the structure of the acoustic field," which is molded by the interference among components that travel along multiple paths. As such, the resolution of MFP is set by "the interference length scales of these propagating multi-path components" [28]. The cross-range extension of the MFP range resolution cell can be expressed as

$$\Delta X \approx \frac{\lambda R}{L}, \tag{3.1}$$

where λ is the wavelength, R represents the range, and L denotes the length of the array [29].

Table 3.1. Matched field processing range resolution at 1500m/s.

	49Hz	166Hz	201Hz	388Hz
$\triangle X_{3000m}[m]$	765.31	225.9	186.57	96.65
$\triangle X_{5000m}[m]$	1275.51	376.51	310.94	161.08

Normal modes are standing waves with horizontal wave numbers k_n as they propagate in range and oscillate in the depth dimension. The depth-dependent mode shapes are defined by the interference between upward and downward propagating plane waves, with vertical wave numbers specified as

$$k_{nz}(z) = \sqrt{k_0^2(z) - k_n^2}, \tag{3.2}$$

where $k_0(z)$ represents the medium wave number $\omega/c(z)$. Both $k_0(z)$ and k_{zn} vary with depth due to variations in the speed of sound at differing ocean depths. The ocean's depth and frequency determine the number of modes a waveguide can support [28]. Several initial MFP studies set simple resolution guidelines for range-independent environments based on mode interference lengths. According to Wilson et al. [30], the smallest mode interference length sets the limit for achievable range resolution. The range interference between two modes aligns with $e^{i(k_n - k_m)r}$, resulting in an interference wavelength in the range of $2\pi/(k_n - k_m)$. Hence, the smallest interference is

$$L_R \approx \frac{2\pi}{max(k_n - k_m)}, \tag{3.3}$$

$$L_R \approx \frac{2\pi}{k_1 - k_M}, \tag{3.4}$$

where k_1 denotes "the wave number for mode 1" and k_M represents "the wave number for mode M," which is "the highest propagating mode" carrying substantial energy [28].

Table 3.2. Matched field processing main lobe width in range at 1500m/s.

	$k_1[m^{-1}]$	$k_M[m^{-1}]$	$L_R[m]$
49Hz	0.2051	0.0598	43.233
166Hz	0.6953	0.0788	10.1917
201Hz	0.8419	0.0937	8.4384
388Hz	1.6252	0.1073	4.1394

We simulated two moving sources with 20 snapshots. Source 1 is the stronger source, located 3km away from the VLA and moving 300m in 20 snapshots. Source 2, the weaker of the two sources, is positioned 2 km further in range than Source 1 and moves a distance of 40 m across 20 snapshots. The grid of the environment simulation is 200m depth and up to 10km in range. The depth resolution is 10m, and the range resolution is 50m. We set the depth of both sources at 60m and selected the range values from 3km (5km) to 2.7km (4.96km) to imitate moving toward the VLA. Because of environmental uncertainty, we randomly draw replicas from a finer grid within the coarser grid. The finer grid's depth resolution is 2m, and the range resolution is 5m.

Bartlett uses the combined SCM averaged over L snapshots. The power ratio between Source 1 and Source 2 (signal to signal ratio (SSR)), denoted by ξ is $\xi = 10^{-3/20}\left\|\hat{K}_1\right\|_{\mathcal{F}}$, meaning that Source 2 has a power level 3dB below that of Source 1. Here, $\mathcal{F}$ represents the Frobenius norm. Following this, the covariance of Source 2 is combined with the covariance of Source 1: $\hat{K} = \hat{K}_1 + \xi\hat{K}_2$ [21].

We extracted sample data between 25 and 55 minutes from the SwellEx-96 data set, comprising a total time interval of 1,800 seconds. With a sampling frequency of 1500Hz and a snapshot length equal to 2^{12}, the frequency interval (or bin width) is 0.3662Hz. Initially, we set the number of snapshots to 3 for exploration, resulting in 219 segments, each containing 3 snapshots and 8.2 seconds. The source moves approximately 20m in each segment with a speed of 2.5 m/s. Source 1 starts from the 125th segment and ends at the 139th segment, simulating a location at 5km and movement of 300m. Source 2 starts and ends at the 24th

segment, located at 3km and moving 40m. We set the SSR to 3dB between Sources 1 and 2.

During this procedure, a time-lagged version of the SWellEX-96 Event S5 data was merged with its original counterpart to simulate a situation with dual source [2], [24], [21]. This resulted in a separation of 2 km between the sources.

CHAPTER 4:
Results

This chapter compares the Bartlett and MVB processors for source localization, focusing on their performance with stationary and moving sources. The Bartlett processor's challenges with multiple frequencies and moving sources are highlighted through simulations, while the MVB excels in sidelobe reduction and an eigenvalue-based approach for superior source identification. The real-world effectiveness of both processors is further validated using the SwellEx-96 data set, especially in scenarios with weak sources overshadowed by stronger ones. The study aims to offer a holistic understanding of these processors, emphasizing their strengths, limitations, and implications in source localization.

4.1 Simulations

First, we illustrate two simulated sources, with Source 1 being 3dB louder than Source 2 at a distance of about 3 and 5km, respectively. Figure 4.1 illustrates the performance results of the Bartlett processor for two stationary sources with a single frequency (166Hz), the average of two frequencies (166 and 201Hz), and the average of multiple frequencies (49, 64, 79, 94, 112, 130, 148, 166, 201, 235, 283, 338, 388Hz). White squares indicate the nominal positions of the sources. The color bar depicts the normalized power in dB with a 15 dB dynamic range. The yellowish color means a higher correlation between data and replica and indicates the source position. A bluish color means less power in that range-depth cell and no source. The plots for a single frequency show high power in many range-depth cells away from the marked source positions.

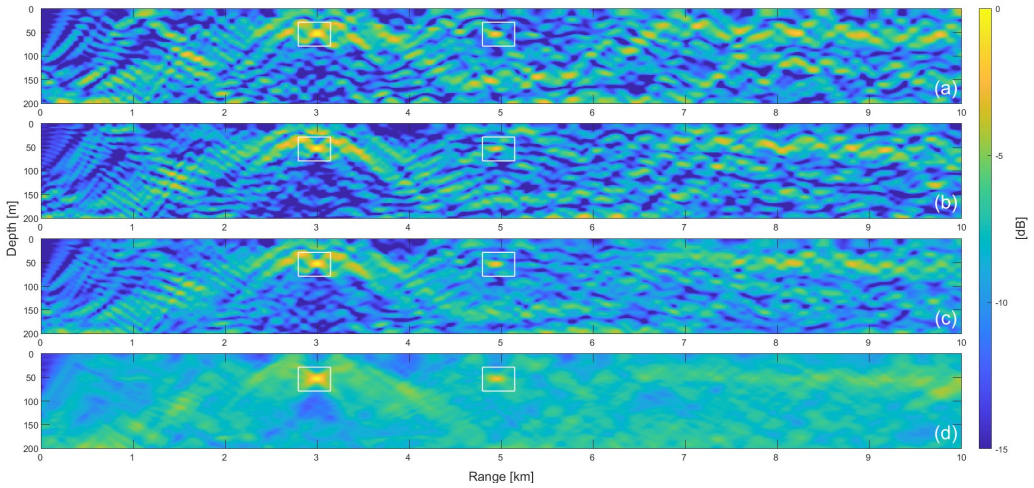

Figure 4.1. Two stationary sources localization simulation with Bartlett: (a) single frequency (166Hz), (b) single frequency (201Hz), (c) the average of two frequencies (166, 201Hz), (d) the average of multiple frequencies (49-388Hz). White squares mark source locations. Source 1, at approximately 3km range, is 3dB louder than Source 2 at approximately 5km range.

Additional simulation results are presented using the multi (13) frequency average. This panel improved source localization when compared to single-frequency panels. That is because the main lobe for all frequencies is in the same range depth cell, and the sidelobes are in different cells.

Figure 4.2 represents Bartlett's performances of moving sources across different frequencies. Source 1 moves 300m, but Source 2 moves 40m, which is assumed to be a stationary source following Table 3.1. Bartlett has high (yellowish) power through many positions for moving sources, which increases Source localization ambiguity. These ambiguities make localizing the correct location of sources complex in plots of the average of two frequencies (166 and 201Hz) and the average of multiple frequencies (49-388Hz). It is challenging to distinguish the weaker source because Bartlett produces several competing sidelobes at similar levels to Source 2. The plot of the average of all frequencies has many competing sidelobes, with a 2 dB difference from the level of Source 2.

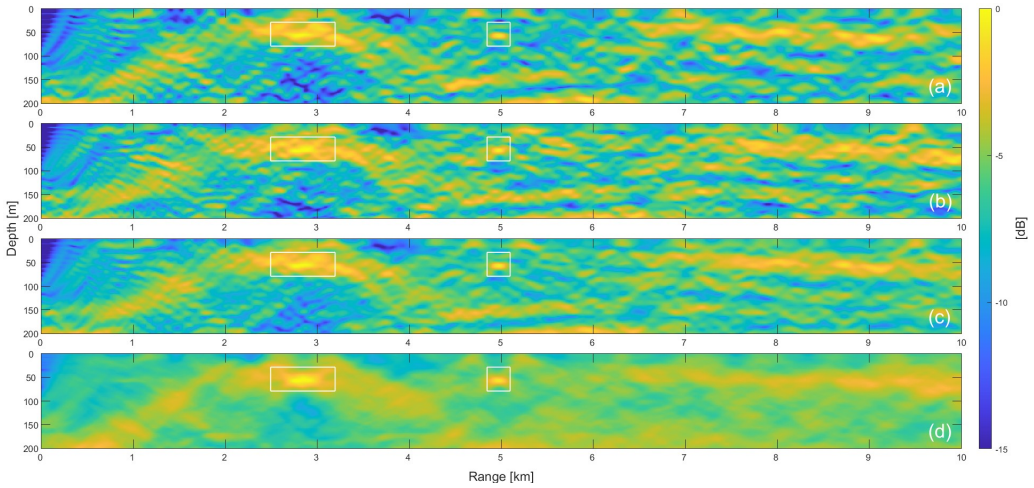

Figure 4.2. As Figure 4.1 but with moving sources. Source 1 (2) moves 300(40)m over the observation interval.

Figure 4.3 contrasts the performances of Bartlett and MVB processors, utilizing a single frequency (166 Hz) for moving sources. The Bartlett processor's performance exhibits localization ambiguities that span the entire surface, with power levels competitive to the actual locations of the sources. In contrast, the plots for MVB distinctly identify Source 1 and Source 2 within eigenvalue 1 and eigenvalue 2, respectively. Furthermore, MVB manifests reduced ambiguity and fewer sidelobes, more closely aligned with the accurate positioning of the sources, as compared to Bartlett, where the sidelobes are at a similar height as the level of Source 2. In localizing Source 2, however, the highest sidelobe height only exhibits a 0.5 dB difference from the level of Source 2, making it difficult to assert that MVB with a single frequency is more accurate than Bartlett. Subsequently, we will explore MVB processing with a single frequency (201 Hz), the average of two frequencies (166 and 201 Hz), and the average of multiple frequencies.

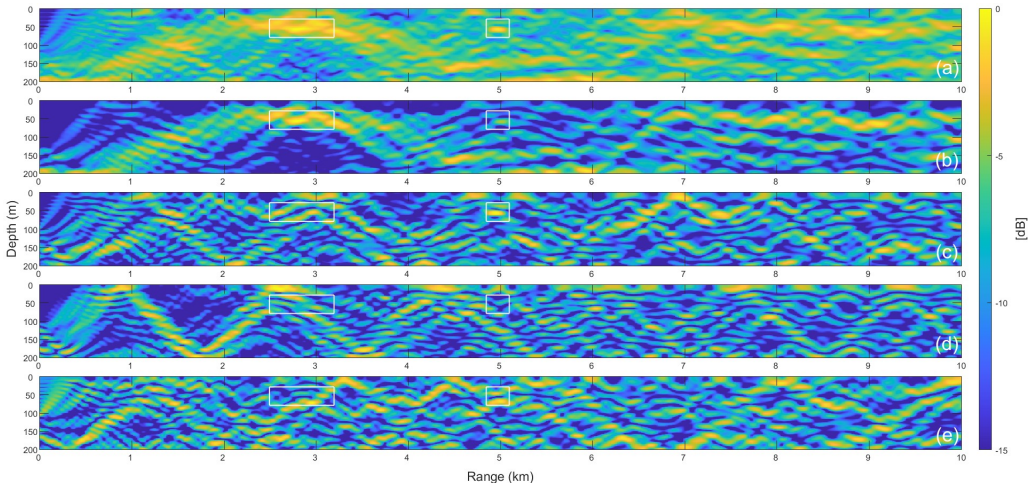

Figure 4.3. Comparison between Bartlett and MVB with single frequency (166Hz): (a) Bartlett Processor, (b) MVB (eigenvalue 1), (c) MVB (eigenvalue 2), (d) MVB (eigenvalue 3), (e) MVB (eigenvalue 4).

Figure 4.4 displays the eigenvalues used in Figure 4.1, incorporating 166 Hz and 201 Hz frequencies. The left plots within these figures illustrate the power of the eigenvalues at 166 Hz, while the right plots reveal the corresponding power at 201 Hz. Eigenvalues 1 and 2 are characterized by significantly greater power than the other eigenvalues, symbolizing the non-moving sources. Figure 4.5 elucidates the eigenvalues used in Figure4.2 in the context of moving sources. This figure conveys that the source movement is distributed across multiple eigenvalues. Despite this dispersion, eigenvalue 1 and eigenvalue 2 still possess more power than the remaining eigenvalues. This distinction plays a crucial role in the MVB processor's operation, as Sources 1 and 2 are precisely located in eigenvalue 1 and 2, respectively.

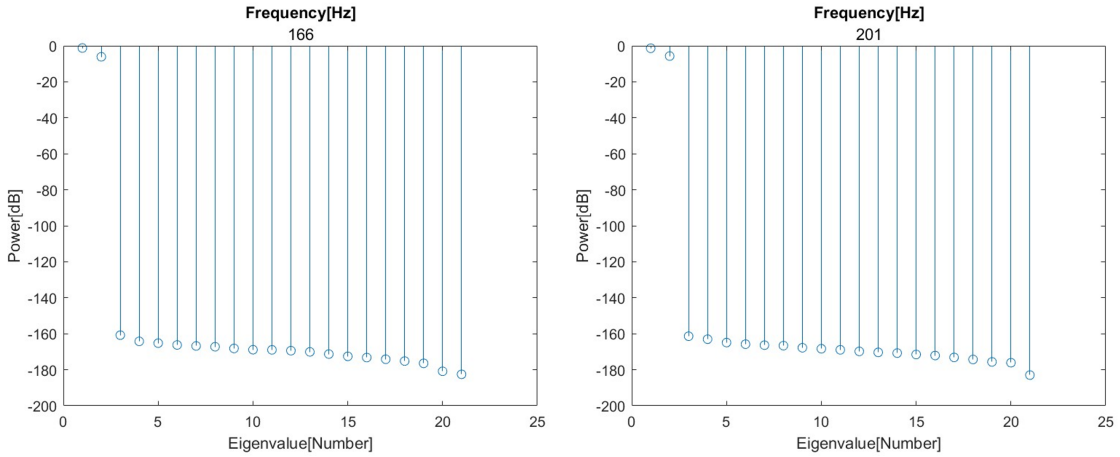

Figure 4.4. Eigenvalues for covariance used in Figure 4.1. The left plot shows the power of eigenvalues at 166Hz, and the right plot illustrates the power of eigenvalues at 201Hz.

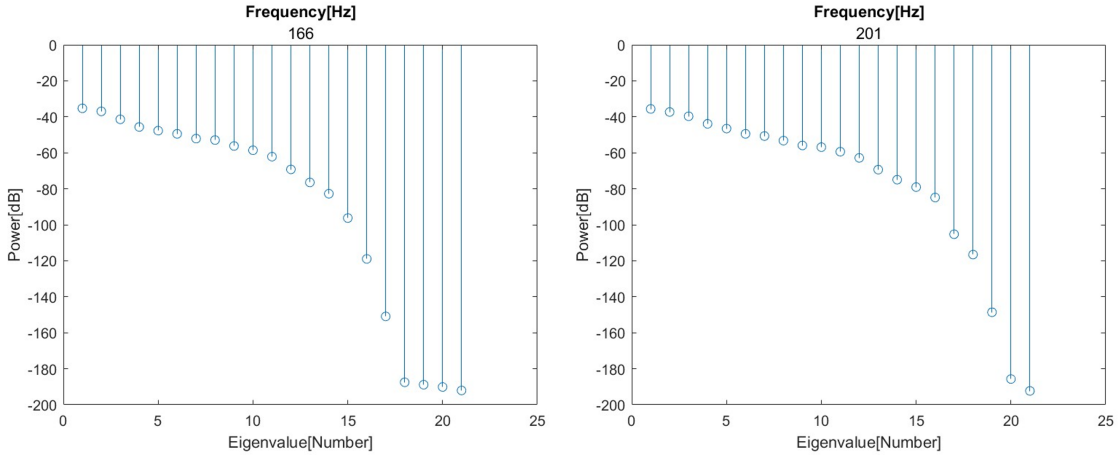

Figure 4.5. Eigenvalues for covariance used in Figure 4.2. The left plot shows the power of eigenvalues at 166Hz, and the right plot illustrates the power of eigenvalues at 201Hz.

Figures 4.6 and 4.7 depict the performance results of MVB using a single frequency (201

Hz) and two frequencies (166 and 201 Hz), respectively. In these representations, Source 1 is discernible in the eigenvalue 1 plot, while Source 2 appears distinctly in the eigenvalue 2 plot. The plot representing the average of two frequencies (166 and 201 Hz) resembles that of the single frequency (201 Hz). A consistent pattern is observed, wherein the weaker source contributes to eigenvalue 2. Nevertheless, there is a discrepancy of 0.8 dB in the highest sidelobe height from the level of Source 2. Given these findings, asserting that MVB surpasses Bartlett definitively remains challenging.

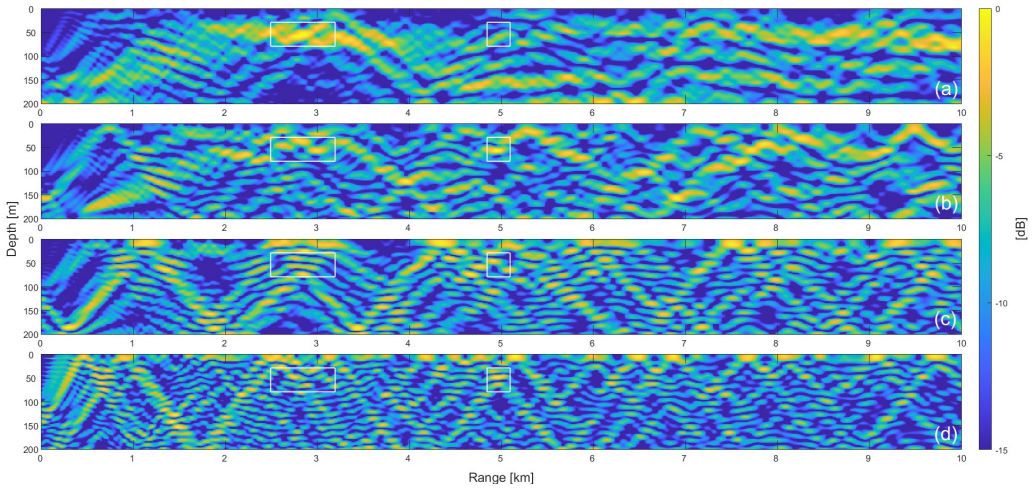

Figure 4.6. MVB with a single frequency (201Hz): eigenvalues (a) 1, (b) 2, (c) 3, (d) 4.

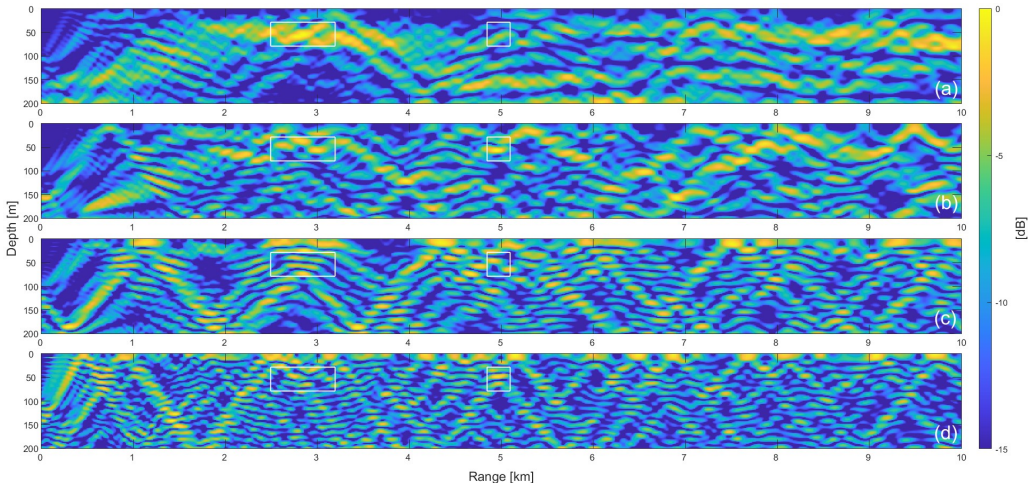

Figure 4.7. MVB with the average of two frequencies (166/201Hz): eigenvalues (a) 1, (b) 2, (c) 3, (d) 4.

According to a study by Booth [4], the sidelobe levels can be reduced by incoherently averaging the processing output across multiple tones, thereby enabling more accurate localization and tracking of the source. Figure 4.8 illustrates the MVB performance when averaging multiple frequencies (49-388 Hz), and this figure reveals an enhancement in performance relative to Figures 4.3, 4.6, and 4.7. In Figure 4.2, Bartlett is observed to have numerous sidelobes, with power levels akin to that of the source within a 5 dB range (from 0 to 5 dB). Conversely, MVB demonstrates substantially lower sidelobes, thereby augmenting source identification and localization performance. A consistent pattern emerges when averaging across frequencies in this moving source scenario: the stronger source primarily influences eigenvalue 1, while the weaker source contributes to eigenvalue 2. Consequently, Source 1 is distinctly observable in the eigenvalue 1 plot, and although Source 2 appears to spread across eigenvalues 2 and 3, averaging over multiple frequencies enhances the processor's performance. Additionally, the highest sidelobe height exhibits a 4 dB difference from the level of Source 2. As a result, the MVB demonstrates superior performance in distinguishing two moving sources compared to Bartlett. This improvement is instrumental in localizing a weaker source that might otherwise be obscured by sidelobes from a stronger source.

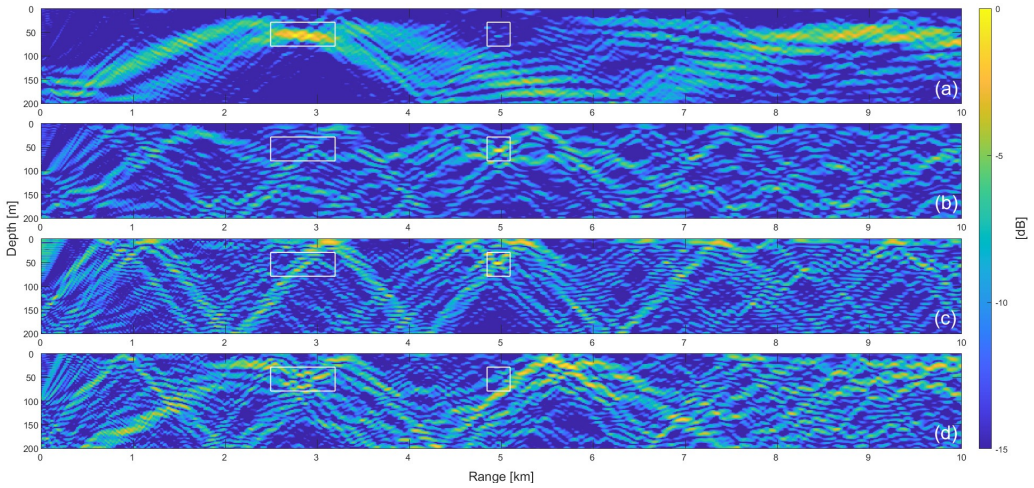

Figure 4.8. MVB with the average of multiple frequencies (49-388Hz) frequencies: eigenvalues (a) 1, (b) 2, (c) 3, (d) 4.

4.2 SWellEX-96 Data Processing

We utilized the SwellEx-96 data set to simulate multi-source scenarios, comparing the Bartlett processor to the MVB processor as in simulation. As depicted in Figure 4.9, we demonstrate the Bartlett performance with two moving sources. The outcomes closely align with our initial simulation results. More pronounced findings were derived from simulations utilizing all frequencies. This enhancement arises from the augmentation of data covariance with the sum of two frequency matrices, reducing sidelobe power for other range depth cells. The Bartlett processor continues to face challenges in identifying the weaker source, however, as it produces multiple competing sidelobes at the levels of Source 2, ranging from 0 to 5 dB. Consequently, the shortcomings in localization persist in the Bartlett processor's output, highlighting the benefits of using the MVB approach in such scenarios.

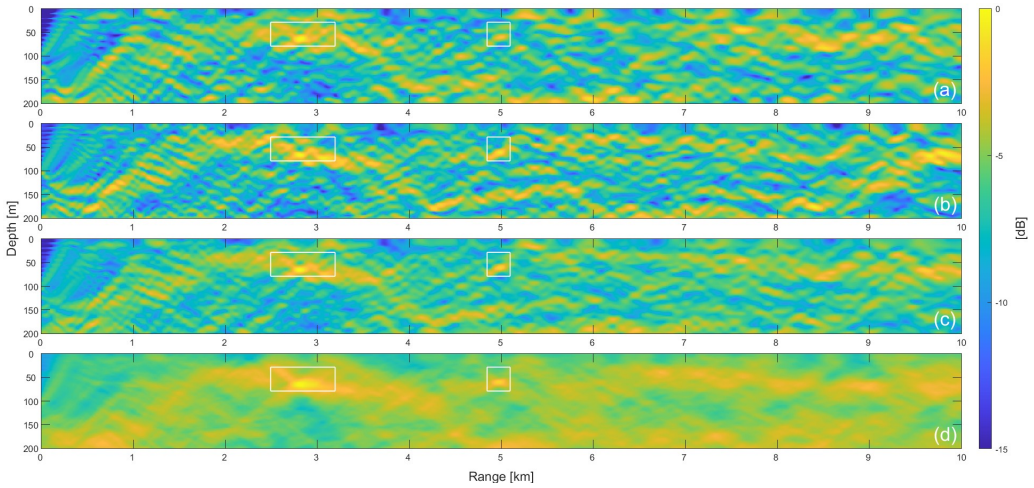

Figure 4.9. Two simulated moving sources using SWellEx-96 data set localization with Bartlett: (a) single frequency (166Hz), (b) single frequency (201Hz), (c) the average of two frequencies (166, 201Hz), (d) the average of multiple frequencies (49-388Hz).

Figures 4.10, 4.11, and 4.12 represent MVB performance using the SwellEx data set with a single frequency (166Hz and 201Hz each) and the average of those two frequencies (166 and 201Hz). The results closely correspond with our simulation findings depicted in the analogous figures. Specifically, Source 1 manifests in the plots for eigenvalue 1, and Source 2 appears distinctively in the plots for eigenvalue 2. This observation underscores a consistent pattern wherein a stronger source contributes to eigenvalue 1 and a weaker source predominantly contributes to eigenvalue 2. An intriguing variation appears when focusing on single frequencies; however, the level of Source 2 in eigenvalue 2 remains the same at 166 Hz or reduces at 201 Hz, while the level of Source 2 actually increases when averaging the two frequencies. This behavior contrasts with the simulation, where the results were similar for a single frequency. It is noteworthy that MVB (when averaging multiple frequencies) presents source location with ambiguity levels comparable to those observed in the simulations, underlining the processor's robustness.

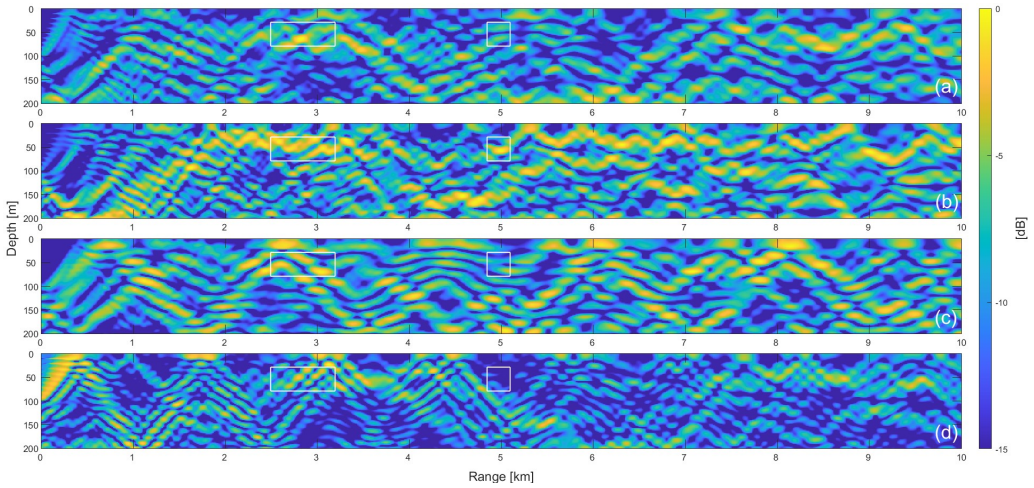

Figure 4.10. MVB a single frequency (166Hz): eigenvalues (a) 1, (b) 2, (c) 3, (d) 4.

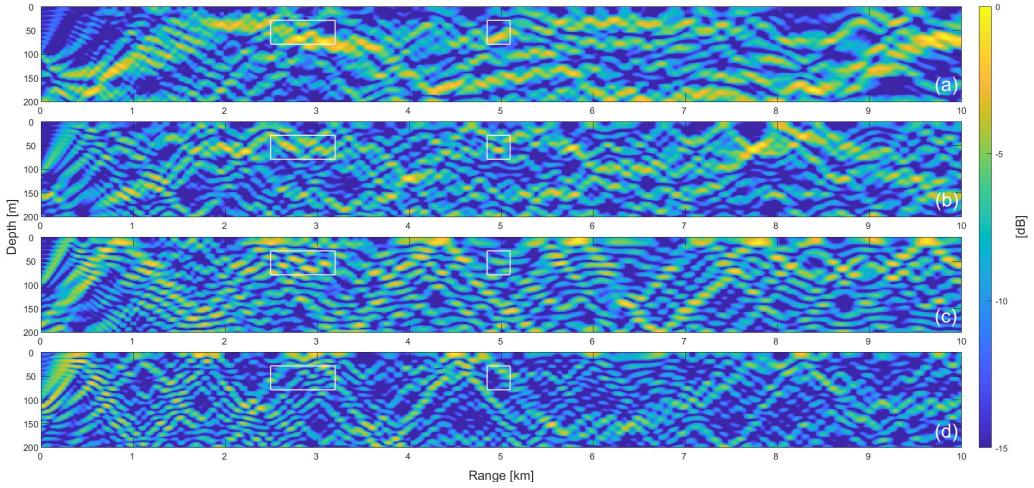

Figure 4.11. MVB with a single frequency (201Hz): eigenvalues (a) 1, (b) 2, (c) 3, (d) 4.

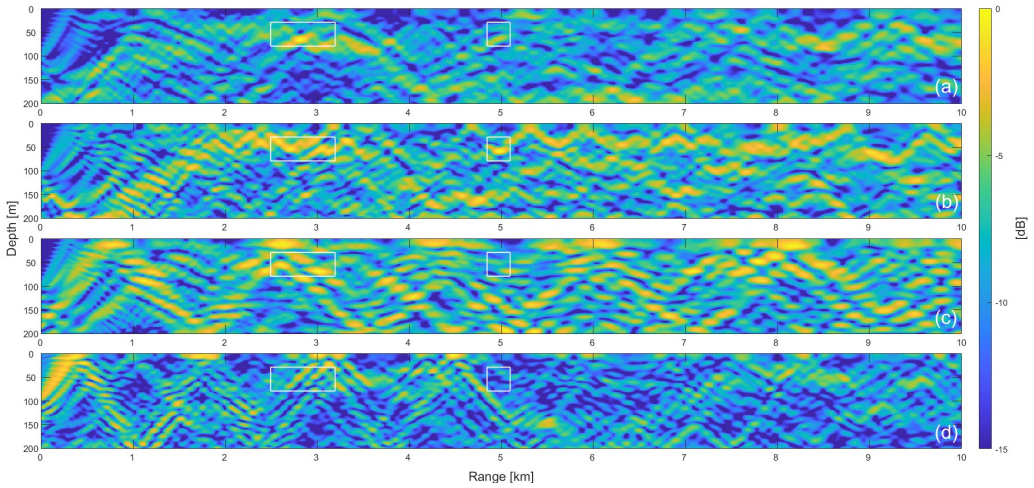

Figure 4.12. MVB with the average of two frequencies (166 and 201 Hz): eigenvalues (a) 1, (b) 2, (c) 3, (d) 4.

Figure 4.13 showcases the performance of MVB on the SwellEx data set across multiple frequencies (49-388Hz). The data results mirror the simulation outcomes but with increased Source 2 localization ambiguity. It appears Source 2 now also has spread to eigenvalues 2 and 3. Additionally, we observe a consistent pattern where a stronger source impacts eigenvalue 1 and a weaker source contributes to eigenvalue 2. As a result, Sources 1 and 2 remain distinguishable within their respective eigenvalue plots, albeit with somewhat less clarity than in the simulation.

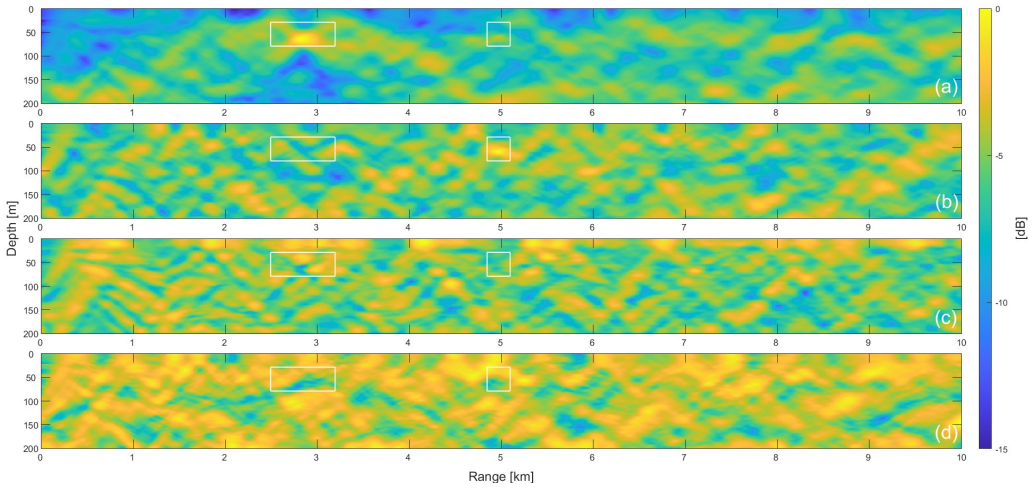

Figure 4.13. MVB with the average of multiple frequencies (49-388Hz): eigenvalues (a) 1, (b) 2, (c) 3, (d) 4.

Figure 4.14 provides the Bartlett and MVB processors' performance for eigenvalues 1 and 2, and the average Bartlett and MVB eigenvalue 2 within a 10 dB dynamic range, specifically examining the SwellEx data set with two simulated moving sources. As the figures illustrate, the Bartlett results are generally in sync with the initial simulation outcomes, and enhancements are apparent when utilizing all frequencies. Despite these strides, the Bartlett processor still struggles to distinguish the weaker source, creating sidelobes similar to the second source's level, with the highest sidelobe height only 0.5 dB below the level of Source 2. In contrast, the level of source 2 in MVB eigenvalue 2 exceeds the highest sidelobe height by 1.5 dB. Consequently, the MVB processor offers slightly improved localization ability compared to the Bartlett processor. Notably, the two approaches' sidelobe patterns are different, while the main lobes are in the same location. Thus, the MVB processor can be used as an additional tool to identify the main lobe. Additionally, by averaging the Bartlett and MVB eigenvalue 2 on the dB-scale, we enhanced the prominence of Source 2, attributed to the distinct sidelobe configurations of each processor. In this scenario, this simple averaging significantly improved the localization of Source 2.

Our research illustrates that while Bartlett and MVB processors share common challenges, particularly in handling weaker sources, the MVB processor can reduce ambiguity, and

its eigenvalue approach can aid in localizing weak signals, especially in complex, multi-source environments. The sidelobe structures for both processors are different. Thus, they can potentially be exploited to identify actual source locations. Given the distinct sidelobe configurations inherent to each processor, there is potential leverage in exploiting these differences to ascertain genuine source locations.

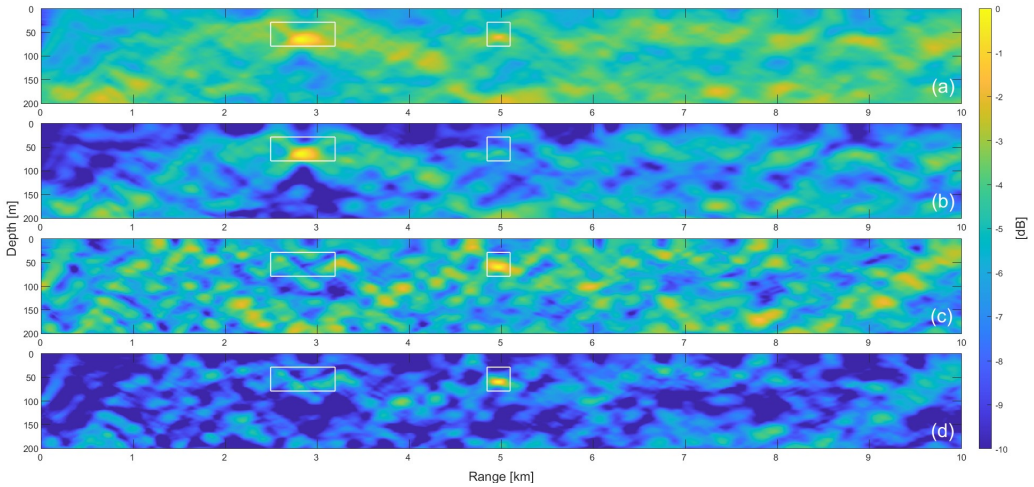

Figure 4.14. Comparison between Bartlett and MVB performance with the average of multiple frequencies (49-388Hz) using SWellEx-96 data set with a 10 dB dynamic range (a) Bartlett, (b) MVB eigenvalue 1, (c) MVB eigenvalue 2, (d) averaged panels (a) and (c) on the decibel scale.

4.3 Conclusion

In this comprehensive evaluation of the Bartlett and MVB processors for source localization, we explored scenarios involving non-moving and moving sources with different frequencies. Utilizing all available frequencies enhanced source localization but posed challenges in distinguishing weaker sources, more so for the Bartlett processor than the MVB processor. Real-world validation through the SwellEx data set provided compelling backing for our simulation results, anchoring the conclusions in practical applications. Despite the noted successes, both processors are limited due to localization ambiguities and high-sidelobes, particularly with moving sources. These challenges underscore the need

for continuous refinement in source localization techniques, reflecting the complexity of real-world scenarios.

The study's broader significance lies in its contribution to the theoretical and practical understanding of source localization processors using multiple frequencies. The insights derived can inform the development of more advanced algorithms adaptable to complex multi-source environments.

Our research contributes to the source localization field by providing a robust, nuanced analysis. We have confirmed existing processors' known strengths and unveiled new avenues for exploration and innovation. The evidence-based support for the multi-frequency MVB processor, in particular, sets it forth as a promising tool for ongoing research and development. The Bartlett processor exhibited localization ambiguities, especially with weaker and moving sources, struggling with multiple competing sidelobes. Conversely, the MVB processor displayed enhanced performance, marked by reduced ambiguity and fewer sidelobes, and used eigenvalues to facilitate a more exact localization of both strong and weak sources.

Multi-frequency averaging emerged as a beneficial strategy for both processors, reducing sidelobe levels and enhancing source localization. This approach was consistent with Booth's study [4] and proved effective in simulations and real-world data scenarios. It is essential, however, to recognize that while MVB generally surpassed Bartlett in the tested scenarios, it lacked challenges. The difference in localization accuracy was marginal in some instances, and one processor's superiority over the other was nuanced. Furthermore, compared to simulations, MVB exhibited increased source localization ambiguity in specific real-world data scenarios, underlining potential limitations.

Further emphasizing our findings, by averaging the Bartlett and MVB eigenvalue 2 on the dB-scale, we significantly improved the prominence of Source 2. This result is credited to the unique sidelobe configurations characteristic of each processor. Though beneficial here, this averaging method's reliability is not investigated exhaustively, yet its position enhancement of Source 2 is significant in this work.

Future directions for this research include further refinement of MVB processing to handle real-world data sets with complex noise environments and multiple sources. Investigating

the synergistic combination of Bartlett and MVB processors in a unified framework might lead to more robust and accurate processors. In conclusion, this study furnishes valuable insights into the complexities of source localization and the comparative capabilities of Bartlett and MVB processors. Although both have unique strengths and weaknesses, the results tilt in favor of MVB, particularly in challenging multi-source situations. The findings lay a solid foundation for future research and technological innovation in source tracking, localization, and analysis.

THIS PAGE INTENTIONALLY LEFT BLANK

List of References

[1] A. B. Baggeroer, W. A. Kuperman, and P. N. Mikhalevsky, "An overview of matched field methods in ocean acoustics," *IEEE Journal of Oceanic Engineering*, vol. 18, no. 4, pp. 401–424, 1993 [Online]. Available: https://doi.org/10.1109/48.262292

[2] K. L. Gemba, W. S. Hodgkiss, and P. Gerstoft, "Adaptive and compressive matched field processing," *The Journal of the Acoustical Society of America*, vol. 141, no. 1, pp. 92–103, Jan. 2017. Publisher: Acoustical Society of America (ASA) [Online]. Available: https://doi.org/10.1121/1.4973528

[3] F. B. Jensen, W. A. Kuperman, M. B. Porter, and H. Schmidt, *Computational Ocean Acoustics*. New York, NY, USA: Springer, 2011 [Online]. Available: https://doi.org/10.1007/978-1-4419-8678-8

[4] N. Booth *et al.*, "Source localization with broad-band matched-field processing in shallow water," *IEEE Journal of Oceanic Engineering*, vol. 21, no. 4, pp. 402–412, 1996.

[5] G. Byun, F. H. Akins, K. L. Gemba, H. C. Song, and W. A. Kuperman, "Multiple constraint matched field processing tolerant to array tilt mismatch," *The Journal of the Acoustical Society of America*, vol. 147, no. 2, pp. 1231–1238, Feb. 2020. Publisher: Acoustical Society of America (ASA) [Online]. Available: https://doi.org/10.1121/10.0000784

[6] A. B. Baggeroer, W. A. Kuperman, and H. Schmidt, "Matched field processing: Source localization in correlated noise as an optimum parameter estimation problem," *Journal of the Acoustical Society of America*, vol. 83, no. 2, pp. 571–587, 1988 [Online]. Available: https://doi.org/10.1121/1.396151

[7] C. S. Clay, "Use of arrays for acoustic transmission in a noisy ocean," *Reviews of Geophysics (1985)*, vol. 4, no. 4, pp. 475–507, 1966 [Online]. Available: https://doi.org/10.1029/RG004i004p00475.

[8] M. J. Hinich, "Maximum-likelihood signal processing for a vertical array," *The Journal of the Acoustical Society of America*, vol. 54, no. 2, pp. 499–503, Aug. 1973 [Online]. Available: https://doi.org/10.1121/1.1913606

[9] H. P. Bucker, "Use of calculated sound fields and matched-field detection to locate sound sources in shallow water," *Journal of the Acoustical Society of America*, vol. 59, no. 2, pp. 368–373, 1976 [Online]. Available: https://doi.org/10.1121/1.380872

[10] R. M. Heitmeyer, R. G. Fizell, and W. B. Moseley, *Full Field Ambiguity Function Processing in a Complex Shallow-Water Environment*. Naval Research Lab Washington DC, USA, 1984.

[11] R. G. Fizell and S. C. Wales, "Source localization in range and depth in an Arctic environment," *The Journal of the Acoustical Society of America*, vol. 78, no. S1, pp. S57–S58, Nov. 1985 [Online]. Available: https://doi.org/10.1121/1.2022889

[12] M. D. Collins, "Generalization of the split-step Padé solution," *Journal of the Acoustical Society of America*, vol. 96, no. 1, pp. 382–385, 1994 [Online]. Available: https://doi.org/10.1121/1.410488

[13] M. D. Collins, L. T. Fialkowski, W. A. Kuperma, and J. S. Perkins, "The multivalued Bartlett processor and source tracking," *Journal of the Acoustical Society of America*, vol. 97, no. 1, pp. 235–241, 1995 [Online]. Available: https://doi.org/10.1121/1.412307

[14] N. O. Booth, A. T. Abawi, P. W. Schey, and W. S. Hodgkiss, "Detectability of low-level broad-band signals using adaptive matched-field processing with vertical aperture arrays," *IEEE Journal of Oceanic Engineering*, vol. 25, no. 3, pp. 296–313, July 2000. Publisher: IEEE [Online]. Available: https://doi.org/10.1109/48.855260

[15] P. Hursky, W. S. Hodgkiss, and W. A. Kuperman, "Matched field processing with data-derived modes," *The Journal of the Acoustical Society of America*, vol. 109, no. 4, pp. 1355–1366, Apr. 2001. Publisher: Acoustical Society of America (ASA) [Online]. Available: https://doi.org/10.1121/1.1353592

[16] W. A. Kuperman and P. Roux, *Underwater Acoustics*. New York, NY: Springer New York, 2014, pp. 157–212 [Online]. Available: https://doi.org/10.1007/978-1-4939-0755-7_5

[17] L. M. Brekhovskikh, *Fundamentals of ocean acoustics*, 3rd ed. (Modern acoustics and signal processing). New York, NY, USA: AIP Press/Springer, 2003.

[18] C. L. Pekeris, *Theory of Propagation of Explosive Sound in Shallow Water*. Geological Society of America, Jan. 1948 [Online]. Available: https://doi.org/10.1130/MEM27-2-p1

[19] R. B. Evans, "A coupled mode solution for acoustic propagation in a waveguide with stepwise depth variations of a penetrable bottom," *The Journal of the Acoustical Society of America*, vol. 74, no. 1, pp. 188–195, 1983.

[20] M. B. Porter, *The KRAKEN normal mode program*. U.S. Department of Commerce, National Technical Information Service, Springfield, VA, USA, 1992.

[21] K. L. Gemba, S. Nannuru, P. Gerstoft, and W. S. Hodgkiss, "Multi-frequency sparse Bayesian learning for robust matched field processing," *The Journal of the Acoustical Society of America*, vol. 141, no. 5, pp. 3411–3420, 05 2017 [Online]. Available: https://doi.org/10.1121/1.4983467

[22] A. Baggeroer and H. Cox, "Passive sonar limits upon nulling multiple moving ships with large aperture arrays," in *Conference Record of the Thirty-Third Asilomar Conference on Signals, Systems, and Computers (Cat. No.CH37020)*. IEEE, 1999, vol. 1, pp. 103–108 vol.1. ISSN: 1058-6393.

[23] H. Cox, "Adaptive beamforming in non-stationary environments," in *Conference Record of the Thirty-Sixth Asilomar Conference on Signals, Systems, and Computers, 2002*. IEEE, 2002, vol. 1, pp. 431–438 vol.1. ISSN: 1058-6393.

[24] K. L. Gemba, S. Nannuru, and P. Gerstoft, "Robust ocean acoustic localization with sparse bayesian learning," *IEEE Journal of Selected Topics in Signal Processing*, vol. 13, no. 1, pp. 49–60, 2019 [Online]. Available: https://doi.org/10.1109/JSTSP.2019.2900912

[25] M. D. Collins, R. N. Baer, and H. J. Simpson, "Experimental testing of the noise-canceling processor," *The Journal of the Acoustical Society of America*, vol. 130, no. 3, pp. 1217–1221, Sep. 2011 [Online]. Available: https://doi.org/10.1121/1.3621059

[26] D. J. Brooker, K. L. Gemba, and L. T. Fialkowski, "Overcoming snapshot-deficient measurements with knowledge-aided approaches," *JASA Express Letters*, vol. 2, no. 5, p. 054804, 05 2022 [Online]. Available: https://doi.org/10.1121/10.0010455

[27] M. P. Laboratory. "The SWellEx-96 experiment" [Online]. Available: http://swellex96.ucsd.edu/index.htm

[28] B. H. Tracey, "Matched field range and depth resolution in range-dependent waveguides," *Acoustic Research Letters Online*, vol. 6, no. 4, pp. 274–279, Oct. 2005 [Online]. Available: https://doi.org/10.1121/1.2006247

[29] H. Cox, R. M. Zeskind, and M. M. Owen, "Robust adaptive beamforming," *IEEE Transactions on Acoustics, Speech, and Signal Processing*, vol. 35, no. 10, pp. 1365–1376, 1987 [Online]. Available: https://doi.org/10.1109/TASSP.1987.1165054

[30] G. R. Wilson, R. A. Koch, and P. J. Vidmar, "Matched mode localization," *The Journal of the Acoustical Society of America*, vol. 84, no. 1, pp. 310–320, 1988.

THIS PAGE INTENTIONALLY LEFT BLANK

Initial Distribution List

1. Defense Technical Information Center
   Ft. Belvoir, Virginia

2. Dudley Knox Library
   Naval Postgraduate School
   Monterey, California